

Learning to Animate Images from A Few Videos to Portray Delicate Human Actions

Haoxin Li^{1*}, Yingchen Yu², Qilong Wu³, Hanwang Zhang¹, Boyang Li¹, Song Bai²

¹Nanyang Technological University ²ByteDance ³National University of Singapore

Abstract

Despite recent progress, video generative models still struggle to animate human actions from static images, particularly when handling uncommon actions whose training data are limited. In this paper, we investigate the task of learning to animate human actions from a small number of videos—16 or fewer—which is highly valuable in real-world applications like video and movie production. Few-shot learning of generalizable motion patterns while ensuring smooth transitions from the initial reference image is exceedingly challenging. We propose FLASH (Few-shot Learning to Animate and Steer Humans), which improves motion generalization by aligning motion features and inter-frame correspondence relations between videos that share the same motion but have different appearances. This approach minimizes overfitting to visual appearances in the limited training data and enhances the generalization of learned motion patterns. Additionally, FLASH extends the decoder with additional layers to compensate lost details in the latent space, fostering smooth transitions from the initial reference image. Experiments demonstrate that FLASH effectively animates images with unseen human or scene appearances into specified actions while maintaining smooth transitions from the reference image. The animated videos can be accessed on the webpage https://lihaoxin05.github.io/human_action_animation/.

1. Introduction

Despite substantial progress [9, 21, 22, 27, 40, 56, 64–66, 69, 76, 78, 82], video generative models still struggle to accurately portray human actions from static images. Even commercial AI video generators, such as Dream Machine¹ from Luma AI and KLING AI² from Kuaishou, encounter difficulty with this task. As shown in Figure 1, both mod-

els fail to animate actions such as balance beam jump or shooting a soccer ball from static images. This difficulty arises from the scarcity of training data that specifically depict the target action. As human actions are diverse and likely follow a long-tailed distribution, many highly recognizable human actions, such as those of a niche sport like balance beam, suffer from limited training data. The data scarcity prevents data-hungry video generative models from effectively learning such actions.

In this paper, we explore the task of learning to animate human actions from a small set of videos. Our aim is to transform a static reference image into a short video of a few seconds, which portrays a specific human action described by a textual prompt. This transformation is learned from a limited dataset containing up to 16 videos for each action class, thereby reducing the need for extensive video data collection. This capability holds the promise to reduce computational cost and broaden the application domains of video generative models; it is particularly valuable for applications like video and movie production, which needs to animate specific actors performing a wide range of actions, yet each action is only used once or twice. Under such use cases, techniques requiring many example videos for each action become cost-ineffective.

Existing image animation methods encounter considerable difficulties with this task. These approaches typically rely on large video datasets for training and primarily focus on preserving the appearance of the reference images [15, 15, 19, 20, 32, 44, 52, 63, 72, 80] or on learning spatial-temporal conditioning controls (e.g., optical flows) to guide image animation [33, 47, 55]. However, these methods become impractical for the few-shot task. When limited to no more than 16 videos, these methods suffer from severe overfitting and fail to learn generalizable motion patterns and object transformations. [68, 81] employ a two-path approach to customize motion from a few videos, but they require training for each reference image for animation, leading to limited flexibility. Although [34, 37, 46, 70] attempt to learn appearance-irrelevant motion patterns from limited data, their models lack explicit supervision for appearance-

*Part of the work is done during an internship at ByteDance.

¹<https://lumalabs.ai/dream-machine>

²<https://www.klingai.com/>

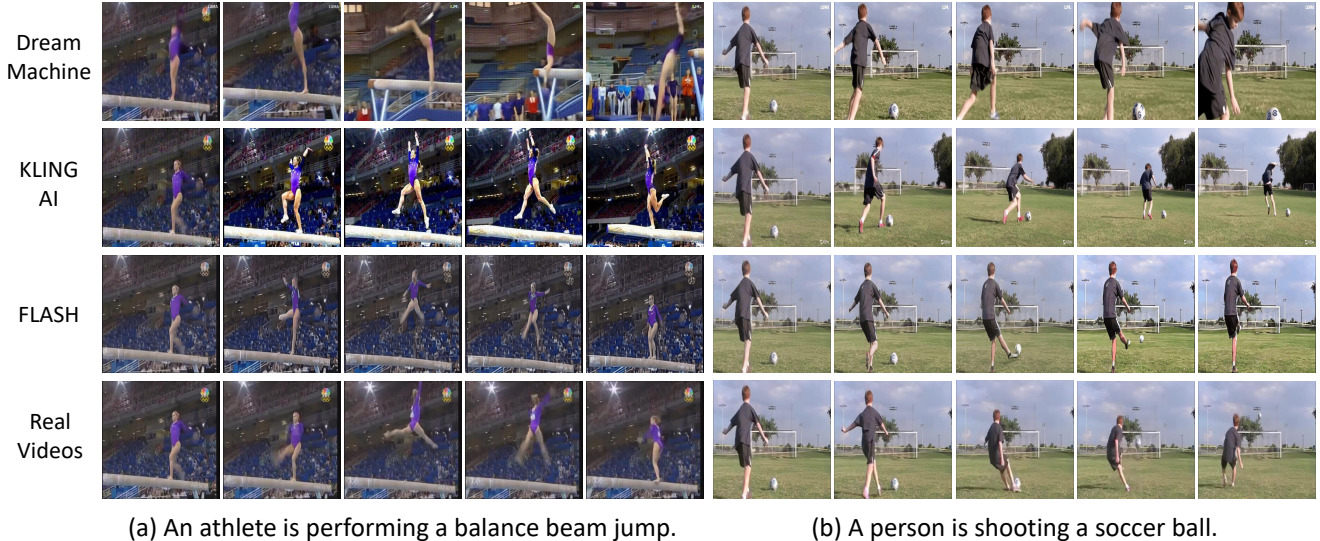


Figure 1. Comparison of animated human action videos produced by Dream Machine, KLING AI, and FLASH (our method). In the balance beam jump action, Dream Machine produces unrealistic, physics-defying movements, whereas KLING AI generates a jump but fails to portray standard jumps on the balance beam. For the soccer shooting action, both Dream Machine and KLING AI struggle to generate the correct shooting motion and the person never kicks the ball away. In contrast, FLASH successfully animate actions that resemble the real-world actions in the last row. We provide additional examples in Figure A1 of Appendix.

general motion, which limits performance.

The main challenge of this few-shot task is learning generalizable motion patterns. The limited number of training videos makes it difficult to learn motion patterns that generalize to diverse appearances. In addition, the initial reference image adds an extra condition, requiring the motion to align with the spatial arrangement of humans or objects in the image to maintain smooth transitions from it. The few-shot learning of motion that generalize to user-provided reference images is more challenging.

To tackle this challenge, we propose FLASH (**F**ew-shot **L**earning to **A**nimate and **S**teer **H**umans), a method for few-shot human action animation. To learn generalizable motion patterns, FLASH devise the Motion Alignment Module to align the motion features and inter-frame correspondence relations between a video and its strongly augmented variant, where the motion remains the same but the appearance differs significantly. By requiring the model to predict the two videos using the two aligned motion patterns, this approach encourages learning motion patterns that can generalize across different appearances, reducing overfitting to the appearance in the limited training data. Additionally, to improve transition smoothness from the reference image, FLASH employs the Detail Enhancement Decoder to propagate the details in the reference image to generated frames, which compensates for the loss of details in the latent space in the decoding process. The overall framework of FLASH is illustrated in Figure 2 (a).

Through experiments on 12 atomic human actions selected from HAA500 [7], we demonstrate that FLASH ac-

curately animates human actions from diverse reference images while maintaining smooth transitions. It outperforms existing image animation methods across various quantitative metrics and human evaluations, showcasing the effectiveness and superiority of FLASH. It also generalizes to non-realistic figures like cartoon characters or humanoid aliens. Our contributions include: (1) We tackle the practical and challenging task of few-shot human action animation, an under-explored area with significant potential for video and film production. (2) We propose FLASH, a framework designed to learn generalizable motion patterns from limited training data. (3) Experiments on 12 atomic human actions validate the effectiveness of FLASH.

2. Related Work

Video Generation. Video generation using diffusion models [25, 57, 58] have notably surpassed methods based on GANs [16], VAEs [36] and flow techniques [5]. Diffusion models for video generation can be broadly classified into two groups. The first group generates videos purely from textual descriptions. These methods extend advanced text-to-image generative models by integrating 3D convolutions, 3D UNets, and temporal attention modules to capture temporal dynamics in videos [2, 21, 26, 27, 56, 65, 82]. To mitigate concept forgetting when training on low-quality videos, some methods use both videos and images jointly for training [4, 27]. Large Language Models (LLMs) contribute by generating frame descriptions [18, 28, 38] and scene graphs [11] to guide the video generation. Trained

on large-scale video-text datasets [1, 6, 73], these methods excel at producing high-fidelity videos. However, they typically lack control over specific frame layouts, such as object positions and human poses. To improve controllability, LLMs are used to predict control signals [39, 42, 43], but these signals typically offer coarse control (*e.g.*, bounding boxes) rather than fine-grained control (*e.g.*, detailed human motion or object deformation).

On top of textual descriptions, the second group of techniques benefit from additional guidance sequences, such as depth maps, motion vectors, optical flows, and bounding boxes [9, 22, 40, 64, 66, 76, 78], which help control motion and frame layouts. Additionally, several techniques use existing videos as guidance to generate videos with different appearances but identical motion patterns [13, 31, 41, 49, 50, 53, 69, 74, 75, 79]. However, these methods cannot create novel videos that share the same motion class with the guidance video but differ in the actual motion, such as human positions and viewing angles, which limits their generative flexibility.

Image Animation. Image animation involves generating videos that begin with a given reference image. Common approaches achieve this by integrating the image features into videos through cross-attention layers [15, 19, 32, 63, 72], employing additional image encoders [20, 67], or incorporating the reference image into noised videos [14, 15, 44, 52, 70, 77]. Another line of methods focuses on learning structural guidance (*e.g.*, motion maps) that aligns with the reference image to guide the generation of subsequent frames [33, 47, 55]. However, these approaches often require extensive training videos to learn motion or structure guidance. [68, 81] employ a temporal path to learn motion patterns from a few videos and a spatial path to learn appearance from a reference image for animation. However, the need for training on each reference image restricts their flexibility. While [34, 37, 46, 70] are similar to our work in learning specific motion patterns from a few videos, they use the reference image as an appearance condition and rely on the model to automatically prioritize motion over appearance. Without explicit supervision for appearance-general motion, their generalizability is still limited. In this paper, we propose FLASH, which learns generalizable motion from only a few videos through explicit supervision for appearance-general motion, and the learned motion can be applied to reference images that differ widely in visual attributes like human positions and texture.

3. FLASH

To learn generalizable motion from a limited set of training videos while maintaining smooth transition from the reference image, we propose FLASH, which builds upon a video diffusion model (see Sec. 3.1) and features two novel components as illustrated in Figure 2. The first is the

Motion Alignment Module, designed to learn robust motion patterns that generalize across different appearances, which will be detailed in Sec. 3.2. The second is the Detail Enhancement Decoder, which propagates details from the reference image to generated frames to enhance transition smoothness, and will be explained in Sec. 3.3.

3.1. Preliminaries

Image Diffusion Models. Latent Diffusion Models (LDM) [54], a leading image generative model, comprises four main components: an image encoder \mathcal{E} , an image decoder \mathcal{D} , a text encoder \mathcal{T} , and a U-Net ϵ_θ . During training, an image $\mathbf{x} \in \mathbb{R}^{H \times W \times 3}$ is first encoded into a latent image $\mathbf{z}_0 = \mathcal{E}(\mathbf{x}) \in \mathbb{R}^{h \times w \times c}$, where h , w and c denote the height, width and number of channels of the latent image, respectively. Next, \mathbf{z}_0 undergoes a pre-defined diffusion process [8, 25] to add noise, resulting in $\mathbf{z}_t = \sqrt{\bar{\alpha}_t} \mathbf{z}_0 + \sqrt{1 - \bar{\alpha}_t} \boldsymbol{\epsilon}_t$, where $\boldsymbol{\epsilon}_t \sim \mathcal{N}(\mathbf{0}, I)$, $t \in [0, T]$ denotes the noising step, and $\bar{\alpha}_t$ denotes the noise strength. The U-Net is then trained to predict the noise $\boldsymbol{\epsilon}_t$ from \mathbf{z}_t . During inference, a latent noise \mathbf{z}_T is drawn from $\mathcal{N}(\mathbf{0}, I)$ and progressively denoised into $\hat{\mathbf{z}}_0$. Finally, the decoder reconstructs the generated image $\hat{\mathbf{x}} = \mathcal{D}(\hat{\mathbf{z}}_0)$.

Video Diffusion Models. The LDM framework can be naturally extended to generate videos. Given a video consisting of N frames $\mathbf{X} = \langle \mathbf{x}^i \rangle_{i=1}^N$, each frame is encoded into a latent frame $\mathbf{z}_0^i = \mathcal{E}(\mathbf{x}^i) \in \mathbb{R}^{h \times w \times c}$. Collectively, all latent frames form a latent video $\mathbf{Z}_0 = \langle \mathbf{z}_0^i \rangle_{i=1}^N \in \mathbb{R}^{N \times h \times w \times c}$ used in the noising and denoising processes. The training loss is defined as:

$$\mathcal{L}_D = \mathbb{E}_{\mathbf{X}, \boldsymbol{\epsilon}_t \sim \mathcal{N}(\mathbf{0}, I), t, y} \left[\|\boldsymbol{\epsilon}_t - \epsilon_\theta(\mathbf{Z}_t, t, \mathcal{T}(y))\|_2^2 \right], \quad (1)$$

where y is the text prompt associated with the video. To capture temporal dynamics in videos, temporal attention layers are integrated into the U-Net [9, 20, 21, 27]. To enhance consistency between frames, the self-attention layers in the U-Net are replaced with cross-frame attention layers [35, 70], in which features from the first frame (the reference frame) are used as the key and value, enabling the appearance of the first frame to be propagated to subsequent frames. In image animation tasks, the noise-free reference image is integrated into the noised latent video [52, 70] to preserve the appearance of the reference image. Further details are in Appendix Sec. A2.1. FLASH inherits all these components of a standard video diffusion model.

3.2. Motion Alignment Module

The Motion Alignment Module directs the model to learn motion that generalizes across various appearances. To achieve this, we force the model to learn consistent motion patterns from a pair of videos with identical motion but different appearances, created using strong data augmentation. We align two motion signals in the U-Net between the video pairs and requires the model to predict both videos using the

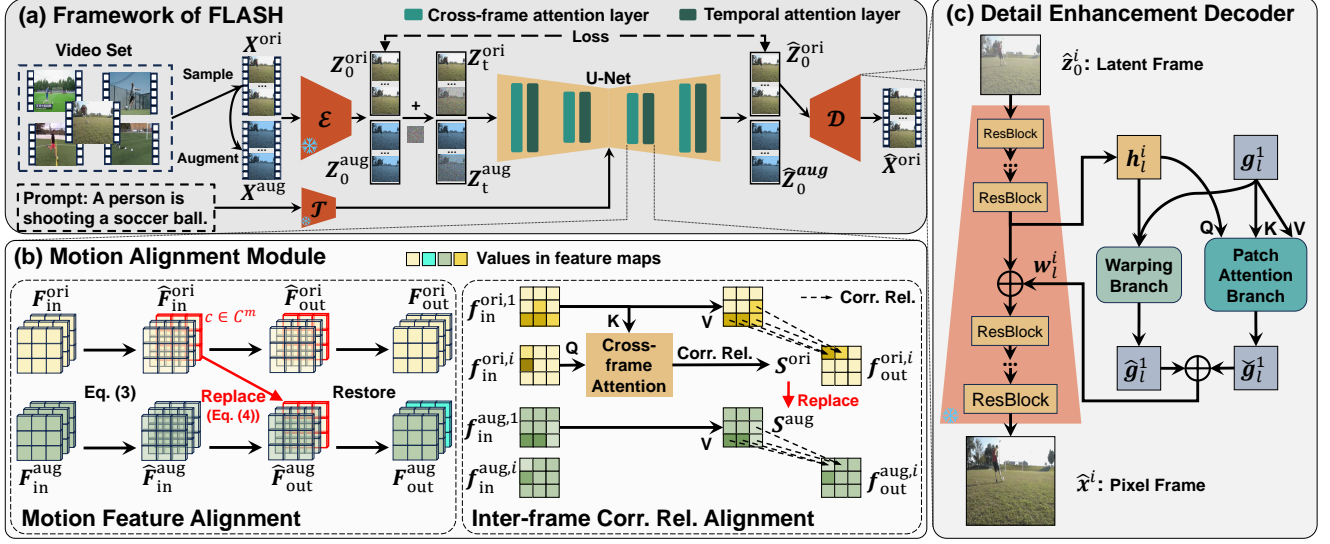


Figure 2. (a) Overview of the FLASH framework. To learn generalizable motion patterns, (b) the Motion Alignment Module aligns motion features and inter-frame correspondence relations (Corr. Rel.) between a training video and its strongly augmented version (see Sec. 3.2). To improve the transition smoothness from the reference image to subsequent frames, (c) the Detail Enhancement Decoder propagates hierarchical details from the reference image into the generated frames (see Sec. 3.3).

same aligned motion signals. This encourages the model to learn general motion patterns across both videos rather than overfitting to appearance patterns in each one. The overall process is depicted in Figure 2 (b) and elaborated in the following sections.

Strongly Augmented Videos. From the original video, X^{ori} , we create a strongly augmented version X^{aug} , which has different appearances but the same motion information. Here we choose the augmentations as Gaussian blur with random kernel sizes and random color adjustments. Details of the augmentations and example augmented videos are in Appendix Sec. A2.2. The overall loss is the diffusion noise prediction, aimed to recover the two videos.

$$\mathcal{L}_D = \mathbb{E}_{X^{\text{ori}}, X^{\text{aug}}, \epsilon_t, t, y} \sum_{v \in \{\text{ori}, \text{aug}\}} \left\| \epsilon_t^v - \epsilon_\theta(Z_t^v, t, \mathcal{T}(y)) \right\|_2^2. \quad (2)$$

For simplicity, we omit the superscripts ori and aug when the same operation is applied to both videos.

Motion Feature Alignment. The purpose of motion feature alignment is to force the model to learn the same motion features from the videos before and after the strong augmentation, which distorts appearance but not motion. We require the model to recover the augmented video from motion features of the original video and the appearance features of the augmented video. This encourages learning of consistent motion features from both videos. We denote the features extracted after a temporal attention layer as $F_{\text{in}} \in \mathbb{R}^{N \times h' \times w' \times c'}$. Since motion is represented by the temporal changes of the features, we remove the static components from F_{in} and normalize it to obtain the dynamic features:

$$\hat{F}_{\text{in}} = \frac{F_{\text{in}} - \mu_{\mathcal{T}}(F_{\text{in}})}{\sigma_{\mathcal{T}}(F_{\text{in}})}, \quad (3)$$

where $\mu_{\mathcal{T}} \in \mathbb{R}^{h' \times w' \times c'}$ and $\sigma_{\mathcal{T}} \in \mathbb{R}^{h' \times w' \times c'}$ are the mean and standard deviation of F_{in} calculated along the temporal

dimension. The standard deviation serves as a normalization factor to reduce the influence of feature scales (e.g., varying brightness in videos). As a result, \hat{F}_{in} becomes independent of static appearance elements and is focused on the changes within the video.

However, motion information is predominantly encoded in a few channels [71], and we need to identify the channels with rich motion information. We quantify the motion information using the standard deviations along the temporal dimension in each channel, which are then averaged across all spatial positions, and the result is denoted as $s \in \mathbb{R}^{c'}$. Channels whose value in s exceed the τ -percentile are identified as motion channels and denoted as the set \mathcal{C}^m . The motion features are thus represented as $\hat{F}_{\text{in}}[c], \forall c \in \mathcal{C}^m$.

We denote the motion features of the original video as $\hat{F}_{\text{in}}^{\text{ori}}[c]$, and those of the augmented video as $\hat{F}_{\text{in}}^{\text{aug}}[c]$. We replace $\hat{F}_{\text{in}}^{\text{aug}}[c]$ with $\hat{F}_{\text{in}}^{\text{ori}}[c]$ as follows:

$$\hat{F}_{\text{out}}^{\text{aug}}[c] \leftarrow \hat{F}_{\text{in}}^{\text{ori}}[c], \quad \forall c \in \mathcal{C}^m. \quad (4)$$

Finally, we restore the features with video-specific mean and standard deviation, $F_{\text{out}}^{\text{ori}} = \hat{F}_{\text{out}}^{\text{ori}} \sigma_{\mathcal{T}}^{\text{ori}} + \mu_{\mathcal{T}}^{\text{ori}}$, $F_{\text{out}}^{\text{aug}} = \hat{F}_{\text{out}}^{\text{aug}} \sigma_{\mathcal{T}}^{\text{aug}} + \mu_{\mathcal{T}}^{\text{aug}}$, which are used in noise prediction $\epsilon_\theta(\cdot)$.

Inter-frame Correspondence Relation Alignment. The purpose of inter-frame correspondence relation alignment is to guide the model to learn the same cross-frame motion between the original and augmented videos. From the attention weights of the original video, we identify spatial correspondence between the first frame and subsequent frames. We require the reconstruction of the augmented video to adopt the same spatial correspondence. This forces the model to learn a general warping strategy across both

videos. Since the video pairs have the same motion but different appearance, the learned warping strategy becomes motion-sensitive and appearance-invariant.

We denote the input features of a cross-frame attention (CFA) layer as $\mathbf{F}_{\text{in}} = \langle \mathbf{f}_{\text{in}}^i \rangle_{i=1}^N \in \mathbb{R}^{N \times h' \times w' \times c'}$. The output features are computed as:

$$\mathbf{F}_{\text{out}} = \text{Softmax} \left(\frac{(\mathbf{Q}\mathbf{W}^{\mathbf{Q}})(\mathbf{K}\mathbf{W}^{\mathbf{K}})^{\top}}{\sqrt{c'}} \right) (\mathbf{V}\mathbf{W}^{\mathbf{V}}) = \mathbf{S}(\mathbf{V}\mathbf{W}^{\mathbf{V}}), \quad (5)$$

where $\mathbf{Q} = \mathbf{F}_{\text{in}}$, $\mathbf{K} = \mathbf{f}_{\text{in}}^1$, $\mathbf{V} = \mathbf{f}_{\text{in}}^1$ are the query, key, and value, respectively, and $\mathbf{W}^{\mathbf{Q}}$, $\mathbf{W}^{\mathbf{K}}$, $\mathbf{W}^{\mathbf{V}}$ are the learnable projection matrices. The key and value are from the first frame of the video. Therefore, \mathbf{S} represents the similarity between the query and the key from the first frame, which implicitly warps the first frame into subsequent frames [45]. Consequently, \mathbf{S} can be interpreted as correspondence relations between spatial locations of the first frame and those of subsequent frames, capturing cross-frame motion.

We denote the inter-frame correspondence relations of the original video and the augmented video as \mathbf{S}^{ori} and \mathbf{S}^{aug} . We replace \mathbf{S}^{aug} with \mathbf{S}^{ori} in the network processing the augmented video. Effectively, this amounts to using \mathbf{S}^{ori} to warp the features of the first frame of the augmented video to produce outputs $\mathbf{F}_{\text{out}}^{\text{aug}}$, which are used to reconstruct the augmented video in $\epsilon_{\theta}(\cdot)$.

3.3. Detail Enhancement Decoder

In LDM, pixel-level details can be distorted when videos are decoded from the latent space, as even slight perturbations within the latent space can lead to noticeable visual artifacts, compromising the intricate details and transition smoothness. To mitigate this issue, we devise the Detail Enhancement Decoder that extends the image decoder \mathcal{D} with additional layers to propagate multi-scale details from the reference image to the generated frames, handling both small and large displacements.

We define the levels of both the encoder and decoder as $l \in \{0, 1, \dots, L\}$, with $l = 0$ representing the pixel space and $l = L$ representing the latent space. At level l , we extract the decoder features of the i -th decoding frame, denoted as \mathbf{h}_l^i , and the encoder features of the reference image, denoted as \mathbf{g}_l^1 . \mathbf{g}_l^1 is then propagated to enhance the details in \mathbf{h}_l^i through two branches, as shown in Figure 2 (c). The **warping branch** retrieves details from nearby areas in \mathbf{g}_l^1 for each spatial position in \mathbf{h}_l^i . It learns the displacements between the two features and warps \mathbf{g}_l^1 into the output $\hat{\mathbf{g}}_l^1$ based on the learned displacements. The **patch attention branch** retrieves details from the global scope of \mathbf{g}_l^1 , complementing the local retrieval of the warping branch. It employs an attention layer with \mathbf{h}_l^i as the query and \mathbf{g}_l^1 as the key and value to produce the output $\tilde{\mathbf{g}}_l^1$. The output features from the two branches are fused using learnable weights \mathbf{w}_l^i : $\tilde{\mathbf{h}}_l^i = \mathbf{h}_l^i + \mathbf{w}_l^i \odot (\hat{\mathbf{g}}_l^1 + \tilde{\mathbf{g}}_l^1)$, where \odot represents element-wise multiplication. The fused features $\tilde{\mathbf{h}}_l^i$ is then passed

to the next level. Through detail propagation at each level for each decoding frame, the details in the generated videos are enhanced. The Detail Enhancement Decoder is trained to retrieve proper details through reconstructing distorted videos to their ground-truth versions. Details can be found in Appendix Sec. A2.3.

4. Experiments

We conduct experiments on 12 actions selected from HAA500 [7]. The actions include single-person actions (push-up, arm wave, shoot dance, running in place, and sprint run), human-object interactions (soccer shoot, drinking from a cup, balance beam jump, canoeing sprint, chopping wood, and ice bucket challenge), and human-human interactions (hugging human). More details about data and implementation are in Appendix Sec. A3.1 and Sec. A3.2.

4.1. Main Results

Metrics. Following [23, 69, 70], we use three CLIP-based metrics: *Text Alignment*, *Image Alignment*, and *Temporal Consistency*, in which higher scores indicate better performance. Following [72], we utilize Fréchet distance to compare generated videos and real ones. To mitigate content bias in the commonly used FVD [62], we adopt *CD-FVD* [12], where a lower distance indicates better performance. To assess the similarity between generated and ground-truth videos in HAA500, we calculate the cosine similarity for each pair of generated and ground-truth videos. We utilize RGB and optical flow to calculate two metrics: *Cosine RGB* and *Cosine Flow*. In these metrics, higher similarities reflect better performance. For all metrics, we report the average results across all test videos. More details are described in Appendix Sec. A3.3.

Baselines. We compare FLASH with several image animation baselines, including the zero-shot training-free image animation model TI2V-Zero [48]; large-scale trained models like SparseCtrl [20], PIA [80] and DynamiCrafter [72]; and motion customization models like DreamVideo [68] and LAMP [70]. More details are described in Appendix Sec. A3.4.

Qualitative Results. We compare the qualitative performance of different methods in Figure 3, excluding TI2V-Zero and SparseCtrl due to their lower quality and space limitations. Animated videos of all methods are available on the webpage. Although PIA, and DynamiCrafter are trained on large-scale video datasets, they still generate unrealistic and disjointed motion that diverges considerably from the correct actions. These results reveal the limitations of large-scale pretrained video generative models in animating uncommon human actions. DreamVideo and LAMP finetune video generative models on a small set of videos containing the target actions. While DreamVideo produces realistic

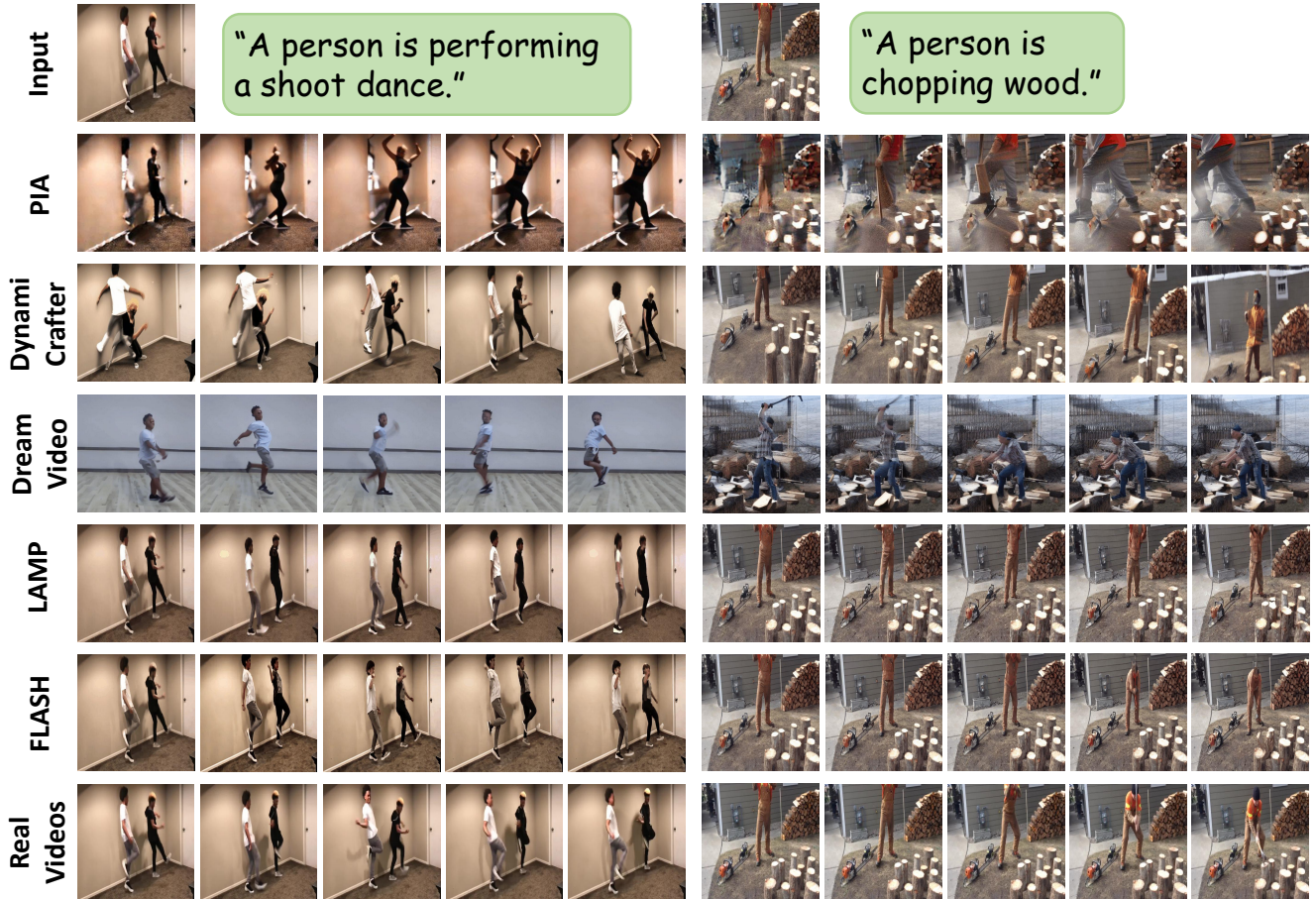


Figure 3. Qualitative comparison of different methods.

actions, it significantly deviates from the reference images. The results indicate that it struggles to adapt motion to different reference images flexibly, because it requires training on each reference image individually. LAMP demonstrates smooth transition from the reference image, but its rendering of the shoot dance displays discontinuities (*e.g.*, disconnected or missing limbs) and it fails to generate the chopping wood action, demonstrating its limitations. In contrast, *FLASH* not only maintains smooth transition from the reference image but also realistically animates the intended actions that resemble real videos, showcasing its effectiveness.

Quantitative Results. We compare *FLASH* with baselines across six metrics in Table 1. The results show that *FLASH* achieves the best overall performance, except in Text Alignment and Image Alignment. This suggests that *FLASH* generates actions with greatest temporal consistency and similarity to real action videos. In terms of Text Alignment, *T12V-Zero* and *DreamVideo* outperform *FLASH*, but both exhibit significantly lower scores on Image Alignment. This implies that while they can generate correct actions, they struggle to animate reference images to portray specified ac-

Table 1. Quantitative comparison of different methods.

Method	Text Alignment (↑)	Image Alignment (↑)	Temporal Consistency (↑)	CD-FVD (↓)	Cosine RGB (↑)	Cosine Flow (↑)
T12V-Zero	23.30	66.75	87.60	1584.30	0.6859	0.5056
SparseCtrl	21.90	60.77	88.54	1627.87	0.6704	0.5663
PIA	23.13	63.58	93.85	1547.61	0.6958	0.6055
DynamiCrafter	22.60	81.71	<u>95.23</u>	1438.01	0.7980	0.6390
DreamVideo	23.77	64.47	93.47	873.76	0.6672	0.6318
LAMP	22.82	77.93	93.92	1260.46	0.8284	0.6989
FLASH	23.02	<u>79.04</u>	95.64	786.39	0.8626	0.7786

tions, as shown in Figure 3. In terms of Image Alignment, *DynamiCrafter* surpasses *FLASH*, but it performs considerably worse on CD-FVD, Cosine RGB, and Cosine Flow. This indicates that although *DynamiCrafter* maintains consistency with the reference images, it fails to generate realistic actions, as also observed in Figure 3.

User Study. Given the potential limitations of the CLIP, I3D, and RAFT models, we conducted a user study to further evaluate the quality of the generated videos. This study was conducted on Amazon Mechanical Turk (AMT), where workers were instructed to select the best generated video

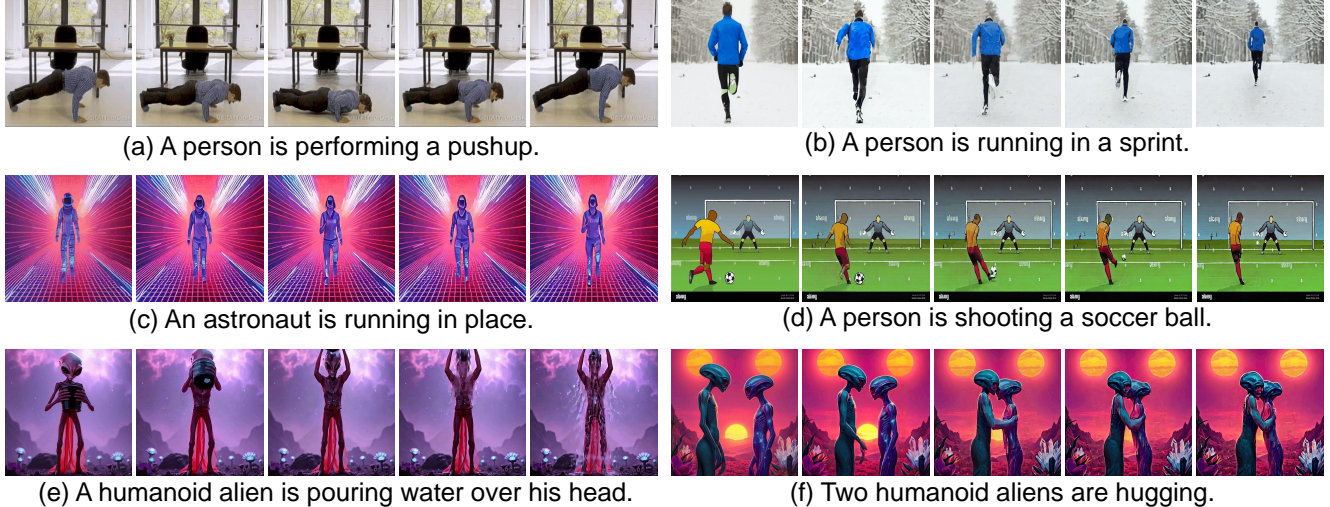


Figure 4. Animated actions generated by FLASH using reference images from the Internet and generated by image generative models.

Table 2. Quantitative ablation studies on different components of FLASH.

Variant	Strong Augmentation	Motion Features Alignment	Inter-frame Correspondence Alignment	Detail Enhancement Decoder	Text Alignment (↑)	Image Alignment (↑)	Temporal Consistency (↑)	CD-FVD (↓)	Cosine RGB (↑)	Cosine Flow (↑)
#1	✗	✗	✗	✗	22.53	77.10	95.43	1023.30	0.8380	0.6806
#2	✓	✗	✗	✗	22.48	76.72	94.91	932.92	0.8398	0.7061
#3	✓	✓	✗	✗	22.64	76.48	95.06	920.39	0.8444	0.7140
#4	✓	✗	✓	✗	22.70	76.31	94.84	938.21	0.8432	0.7172
#5	✓	✓	✓	✗	22.52	76.35	95.01	906.31	0.8446	0.7224
#6	✓	✓	✓	✓	22.77	76.22	95.31	908.39	0.8451	0.7233

from a set of candidates. For each action, we randomly select 4 different reference images for evaluation. Control questions were included to identify random clicking, and only answers from workers who correctly answered the control questions were considered valid. More details are described in Appendix Sec. A4.1. Out of 366 valid responses, FLASH was preferred in 67% of the response, significantly outperforming the next best models, Dynamicrafter (14%) and LAMP (12%). These results indicate that FLASH produces videos of the highest quality.

Generalization to Internet and Generated Images. To assess the generalization capability of FLASH beyond the HAA500 dataset, we tested it on images sourced from the Internet and those generated by Stable Diffusion 3 [10]. As shown in Figure 4, FLASH successfully animated a variety of scenes, including a person doing a pushup in an office and running on snow. It also adapted to unrealistic scenarios, such as an astronaut running in place within a virtual space and a cartoon character shooting a soccer ball. Additionally, FLASH can animate generated images, such as a humanoid alien pouring water over his head, two humanoid aliens hugging. More animated videos are available on the webpage. These results highlight FLASH’s strong generalization ability across a broad spectrum of reference images.

4.2. Ablation Studies

We conducted ablation studies on four actions: sprint run, soccer shoot, canoeing sprint, and hugging human. The quantitative and qualitative results are presented in Table 2 and Figure 5, respectively. Variant #1 serves as the baseline, excluding both the Motion Alignment Module and the Detail Enhancement Decoder. Variant #2 uses only strongly augmented videos without any alignment technique. Variants #3, #4, and #5 progressively incorporate motion feature alignment, inter-frame correspondence relation alignment, and both, respectively. Lastly, Variant #6 builds upon Variant #5 by incorporating the Detail Enhancement Decoder.

Comparing the quantitative results of Variants #1 and #2, we observe that Variant #2 improves CD-FVD, Cosine RGB, and Cosine Flow, albeit with a slight decrease in CLIP scores. Qualitative results show that Variant #2 improves the fidelity of the generated actions. For example, in the soccer shooting action, the person’s legs tend to disappear as the action progresses in Variant #1; however, Variant #2 preserves the leg movements. These results suggest that using augmented videos improves the quality of motion.

Comparing the quantitative results of Variant #2 with Variants #3, #4, and #5, we find that Variants #3, #4, and

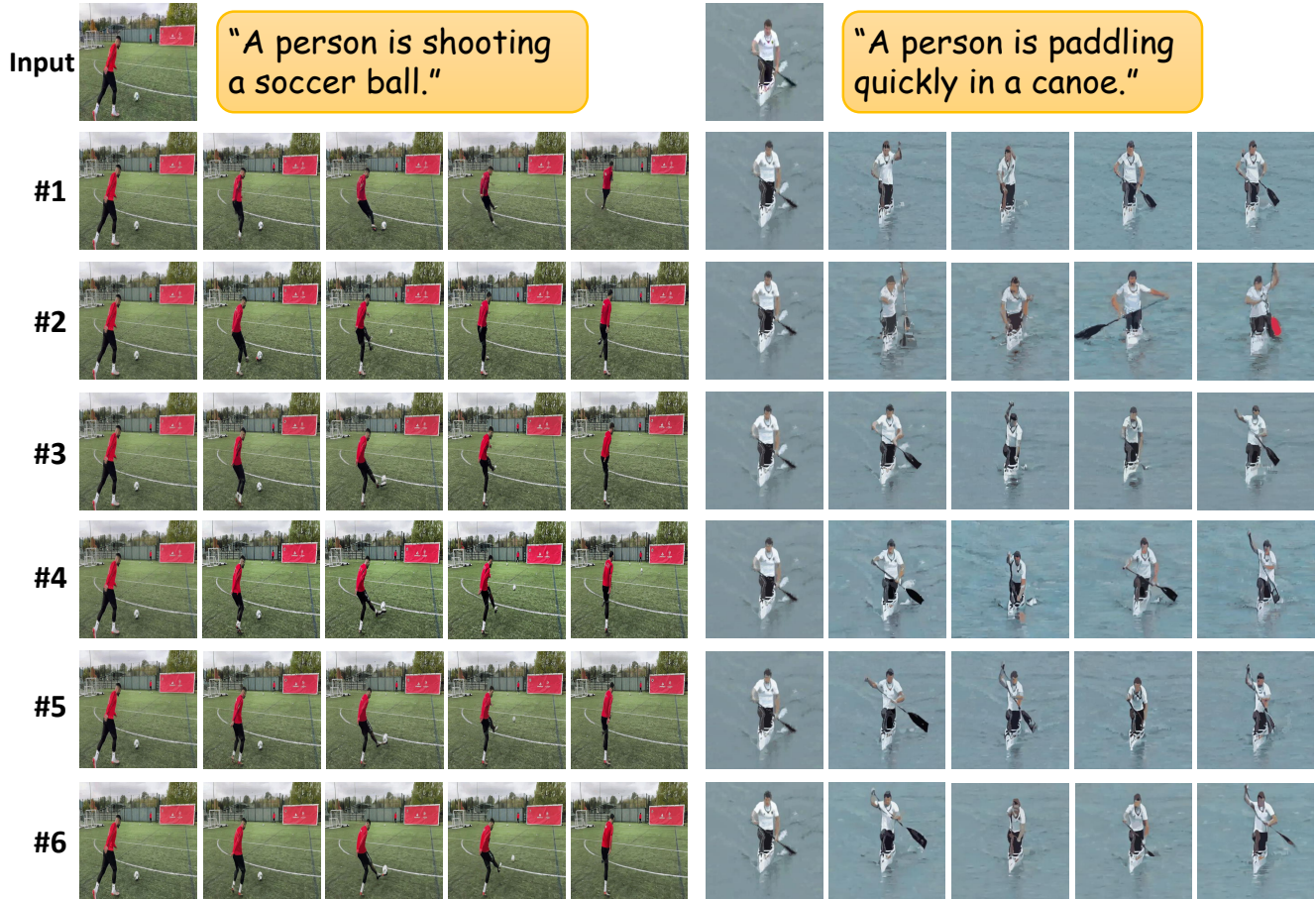


Figure 5. Qualitative ablation study on different components of FLASH. #1: baseline model, #2: model trained with only strongly augmented videos, #3: with motion feature alignment, #4: with inter-frame correspondence alignment, #5: with both alignments, #6: full model with Motion Alignment Module and Detail Enhancement Decoder. See Table 2 for the correspondence of each variant.

#5 improve CD-FVD, Cosine RGB, and Cosine Flow. Both Variants #3 and #4 enhance the Cosine RGB, and Cosine Flow. When combined, Variant #5 yields further enhancements in cosine similarity and a 25-point improvements in CD-FVD, without a noticeable drop in CLIP scores. Qualitative results also indicates improved fidelity in Variants #3, #4, and #5. For instance, motion in Variant #2 appears unrealistic in both actions. In the soccer shooting action, the person’s foot didn’t touch the soccer ball, and the leg appears disconnected in some frames. In the canoe paddling action, the hand positions on the paddle are inconsistent across frames. However, these issues are largely mitigated in Variants #3, #4, and #5. These results demonstrate the effectiveness of the Motion Alignment Module in learning accurate motion. By providing explicit guidance for learning appearance-general motion, the module directs the model toward generalizable motion, thereby improving the quality of the generated videos.

Comparing the quantitative results of Variant #5 and Variant #6, we observe that Variant #6 noticeably improves

Text Alignment and Temporal Consistency without substantially affecting CD-FVD, Cosine RGB, or Cosine Flow. Qualitatively, Variant #6 enhances some details (*e.g.*, the soccer ball in certain frames in the soccer shooting action) and reduces noise in generated frames. These results suggest that the Detail Enhancement Decoder could compensate for action related details in generated frames, leading to better temporal consistency and alignment with the action descriptions. Since the decoder operates on a frame-by-frame manner without considering inter-frame relations, it has minimal impact on motion patterns, resulting in slight changes on CD-FVD, Cosine RGB, and Cosine Flow.

In Appendix Sec. A4.2, we show that the Motion Alignment Module improves performance across different few-shot settings (*i.e.*, 8 or 4 videos per action class) and benefits from joint training across multiple action classes. Additionally, we provide ablation studies analyzing the effects of hyper-parameters in the Motion Alignment Module and the branches of the Detail Enhancement Module. Limitations are discussed in Appendix Sec. A5.

Learning to Animate Images from A Few Videos to Portray Delicate Human Actions

Appendix

The Appendix is structured as follows:

- Section A1 includes supplementary examples comparing videos generated by commercial AI video generators.
- Section A2 elaborates on the details of FLASH.
- Section A3 describes detailed experimental setups.
- Section A4 provides more experimental results.
- Section A5 discusses the limitations of FLASH.
- Section A6 presents the Ethical Statement.
- Section A7 concludes this paper.

A1. Comparison of videos generated by commercial AI video generators

In Figure A1, we show two additional examples of human action videos generated by Dream Machine, KLING AI, and FLASH. It can be observed that Dream Machine and KLING AI fail to animate these two actions accurately. The generated videos are available on the webpage.

A2. More Details of FLASH

A2.1. Preliminaries

Temporal Attention Layers. To capture temporal dynamics in videos, temporal attention layers are introduced into the U-Net [9, 20, 21, 27]. In a temporal attention layer, the input features $\mathbf{F}_{in} \in \mathbb{R}^{N \times h' \times w' \times c'}$ are first reshaped to $\tilde{\mathbf{F}}_{in} \in \mathbb{R}^{B \times N \times c'}$, where $B = h' \times w'$. Here, the features at different spatial locations are treated as independent samples. Temporal position encoding are then added, and a self-attention layer is applied to transform $\tilde{\mathbf{F}}_{in}$ into $\tilde{\mathbf{F}}_{out} \in \mathbb{R}^{B \times N \times c'}$. Finally, $\tilde{\mathbf{F}}_{out}$ is reshaped back to $\mathbf{F}_{out} \in \mathbb{R}^{N \times h' \times w' \times c'}$ as output features. The temporal attention layer integrates information from different frames for each spatial location, enabling the learning of temporal changes.

Cross-frame Attention Layers. To enhance temporal consistency across generated frames, cross-frame attention layers are utilized to replace self-attention layers [35, 70]. While self-attention layers use features from all frames as key and value, cross-frame attention layers restrict key and value to the features from the first frame or the previous frame. This approach preserves the appearance of objects and background from the first frame or the previous frame, improving temporal consistency in the generated videos.

Noise-Free Frame Conditioning. To preserve the appearance of the reference image in the image animation task, the noise-free latent reference image is integrated into the

U-Net input [52, 70]. During training, the first latent frame remains noise-free, while noise is added only to subsequent latent frames throughout the noising process. Specifically, at the noising step t , the latent video $\mathbf{Z}_t = \langle z_t^i \rangle_{i=1}^N$ is modified to $\tilde{\mathbf{Z}}_t = \langle z_0^1, z_t^2, \dots, z_t^N \rangle$, where z_t^i is replaced by z_0^1 , which is noise-free. During inference, a sample \mathbf{Z}_T is drawn from $\mathcal{N}(\mathbf{0}, I)$, and z_T^1 is substituted with $z_0^1 = \mathcal{E}(I)$, where I is the user-provided reference image. The modified latent video $\tilde{\mathbf{Z}}_T = \langle z_0^1, z_T^2, \dots, z_T^N \rangle$ is then used for denoising. This technique effectively carries over the features from the first frame to subsequent frames, ensuring that the appearance of the reference image is preserved in the generated video.

FLASH adopts these components as its base video diffusion model and designs a motion alignment module and a detail enhancement decoder on top of it.

A2.2. Motion Alignment Module

Strongly Augmented Videos. To create a strongly augmented version of an original video, we sequentially apply Gaussian blur and random color adjustments to the original video. This process is designed to preserve the original motion while altering the appearance uniformly across all frames.

- Gaussian blur: A kernel size is randomly selected from a predefined range, as specified in Sec. A3.2. This kernel size is used to apply Gaussian blur consistently to every frame of the original video, ensuring a uniform level of blur throughout.
- Random color adjustments: After applying Gaussian blur, we randomly adjust the brightness, contrast, saturation, and hue of the video. For each property, an adjustment factor is randomly chosen from its respective predefined range, detailed in Sec. A3.2. The adjustment with the chosen factor is applied uniformly across all frames to maintain consistent color alterations without introducing cross-frame inconsistencies. We implement the random color adjustments using the *ColorJitter* function in PyTorch.

By applying these augmentations with consistent parameters across all frames, the augmented video retains the motion in the original video while showing altered appearances. Figure A2 presents examples of strongly augmented videos. These augmented videos exhibit considerable differences from the original ones in aspects such as the background and the actors' clothing. However, the motion from the original videos is preserved.



Figure A1. Comparison of human action videos generated by Dream Machine, KLING AI, and FLASH (our method). For the shoot dance action, both Dream Machine and KLING AI produce unrealistic movements that defy physical laws. In the Ice Bucket Challenge action, neither Dream Machine nor KLING AI accurately captures the motion of pouring ice water from the bucket onto the body. In contrast, FLASH successfully generates both actions with a higher fidelity to the real movements, as shown in the last row. Human faces are anonymized for privacy protection.

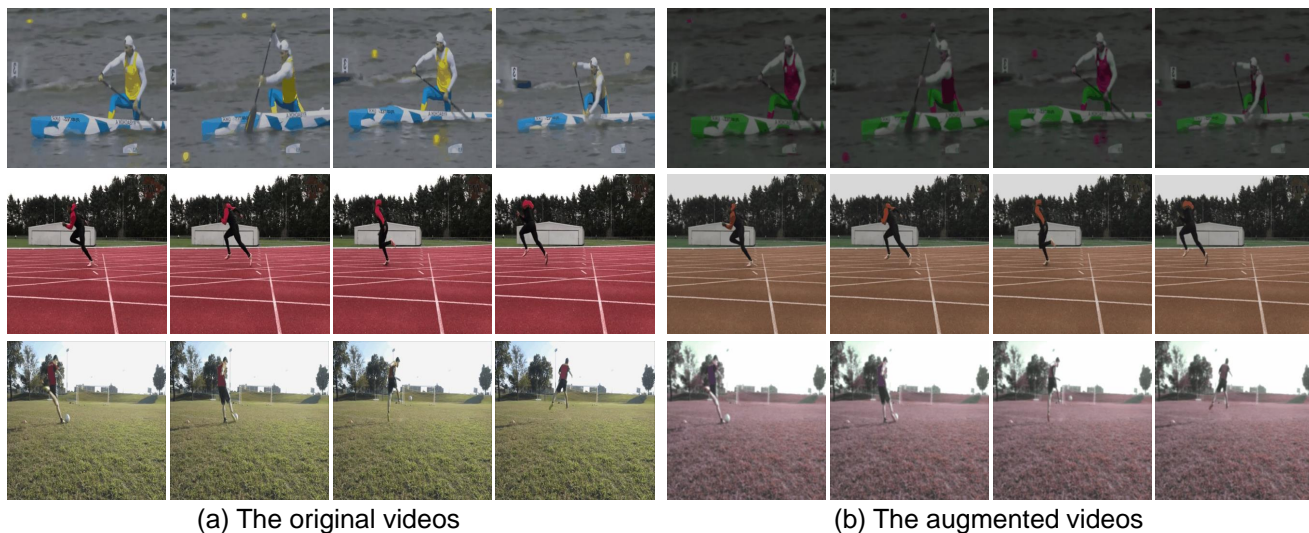


Figure A2. Examples of three original videos alongside their corresponding strongly augmented videos.

A2.3. Detail Enhancement Decoder

In LDM, pixel-level details can be distorted when videos are decoded from the latent space, as even slight perturbations within the latent space can lead to noticeable visual artifacts, compromising the intricate details and transition smoothness. To mitigate this issue, we devise the Detail Enhancement Decoder that extends the image decoder \mathcal{D} with additional layers to propagate multi-scale details from the reference image to the generated frames. Given that motion

between the first frame and subsequent frames can vary, the Detail Enhancement Decoder is designed with two branches to capture details from both small and large displacements, addressing these two different types of motion.

We define the levels of both the encoder and decoder as $l \in \{0, 1, \dots, L\}$, with $l = 0$ representing the pixel space and $l = L$ representing the latent space. At level l , we extract the decoder features of the i -th decoding frame, denoted as h_l^i , and the encoder features of the reference image,

denoted as g_l^1 . We interpolate g_l^1 to match the spatial size of h_l^i and use a fully connected layer to adjust g_l^1 to the same number of channels as h_l^i , resulting \tilde{g}_l^1 as the input of the following two branches, as illustrated in Figure 2 (c) of the main paper.

Warping Branch. This branch aims to retrieve details from nearby areas in \tilde{g}_l^1 for each spatial position in h_l^i . It takes the channel-wise concatenation of h_l^i and \tilde{g}_l^1 as input and applies four convolution layers to estimate motion displacements from h_l^i to \tilde{g}_l^1 . These displacements determine the sampling positions in \tilde{g}_l^1 . By warping \tilde{g}_l^1 based on the sampling positions, the branch outputs \hat{g}_l^1 .

Patch Attention Branch. This branch retrieves details from the global scope of \tilde{g}_l^1 , complementing the local retrieval in the warping branch. It begins by dividing both h_l^i and \tilde{g}_l^1 into patches and transforming each patch into features through a fully connected layer. A cross-attention layer is then applied, using the patch features of h_l^i as the query and the patch features of \tilde{g}_l^1 as the key and value. The output features \tilde{g}_l^1 is a weighted patch combination of \tilde{g}_l^1 .

Feature Fusion. To control the amount of detail added to h_l^i , a two-layer convolution network is used to learn the fusion weights. The network takes the channel-wise concatenation of h_l^i and \tilde{g}_l^1 as input and outputs the fusion weights w_l^i , which has the same spatial size as h_l^i . The fusion is then performed as:

$$\tilde{h}_l^i = h_l^i + w_l^i \odot (\hat{g}_l^1 + \tilde{g}_l^1). \quad (6)$$

The resulting feature \tilde{h}_l^i is then passed to level $l - 1$. The details in the generated frames are enhanced through the hierarchical detail propagation in each level.

Learning to Reconstruct Distorted Videos. We train the Detail Enhancement Decoder to retrieve proper details through reconstructing distorted videos to match their ground-truth versions. During training, we first extract g_l^1 using the first frame of a training video. Next, we intentionally distort the video using random Gaussian blur, random color adjustments on 80% of the randomly selected regions, and random elastic transformations. The distorted video is then encoded into a latent video. The decoder is trained to reconstruct the ground-truth video from the distorted latent video and the extracted feature g_l^1 of the first frame, using MSE loss. This approach encourages the decoder to retrieve relevant details from the reference image to compensate for distorted details in the latent videos.

The details of video distortions are as follows: The random Gaussian blur and random color adjustments follow the implementations described in Sec. A2.2. However, the random color adjustments here differ in that they are applied to only 80% of randomly selected regions rather than to all regions. This modification is intentional, as the goal is to

create distorted videos that simulate the perturbations in latent videos, rather than to maintain consistent color changes as in Sec. A2.2. For random elastic transformations, displacement vectors are generated for all pixels based on random offsets sampled from a predefined range (detailed in Sec. A3.2) and are then used to transform each pixel accordingly. We implement the random elastic transformations using the *ElasticTransform* function in PyTorch.

A3. Experiment Details

A3.1. Data

We conduct experiments on 12 actions selected from the HAA500 dataset [7], which contains 500 human-centric atomic actions, each consisting of 20 short videos. The selected actions include single-person actions (push-up, arm wave, shoot dance, running in place, and sprint run), human-object interactions (soccer shoot, drinking from a cup, balance beam jump, canoeing sprint, chopping wood, and ice bucket challenge), and human-human interactions (hugging human).

Training videos. For each selected action, we use 16 videos from the training split in HAA500 for training. We manually exclude videos that contain pauses or annotated symbols in the frames. Each action label is converted into a natural sentence as the action description; for example, the action label “soccer shoot” is converted to “a person is shooting a soccer ball.”

Similarity between videos in the same action class.

Videos within the same action class do not necessarily share similar visual characteristics, such as scenes, viewing angles, or shot types (*e.g.*, close-up or wide shot), as shown in the examples in Figure A3.

Testing images. For each selected action, we use the first frames from the 4 testing videos as testing images. Additionally, we search online for 2 human images depicting a person beginning the desired action as additional testing images.

A3.2. Implementation Details

We use AnimteDiff [22] as the base model, initializing all parameters with its pretrained weights. The spatial resolution is set to 512×512 , and the video length is set to 16 frames.

Training of U-Net. We combine features from the first and current frames as keys and values in the cross-frame attention layers. As in [52, 70], we apply noise-free first-frame conditioning (see Supplementary Material Sec. A2.1 for details). Following [30, 46], we redefine the sampling probability distribution to prioritize earlier denoising stages. In the motion alignment modules, we set τ to 90 and apply motion feature alignment after each temporal attention layer in



Figure A3. Similarity between videos in the same action class. The first row presents three videos depicting the action canoeing sprint, and the second row showcases three videos illustrating the action push-up.

the U-Net. Inter-frame correspondence relation alignment is applied to 50% of the cross-frame attention layers, selected randomly. For simplicity, we replace Q and K of the augmented video with those of the original video when calculating S , instead of directly replacing S . Gaussian blur is applied with a randomly sampled kernel size between 3 and 10. Color adjustments modify brightness, saturation, and contrast by random factors between 0.5 and 1.5, and modify hue by a random factor between -0.25 and 0.25. Before applying strong augmentations to the original video, we first perform random horizontal flipping and random cropping on the original video. We only train the temporal attention layers and the key and value projection matrices of other attention layers. The learning rate is set to 5.0×10^{-5} , with training conducted for 20,000 steps.

Training of Detail Enhancement Decoder. The patch size in the Patch Attention Branch is set to 2. For video distortion, Gaussian blur is applied with a random kernel size between 3 and 10. Color adjustments use random factors for brightness, saturation, and contrast between 0.7 and 1.3, and a random factor for hue between -0.2 and 0.2. Elastic transformation displacement strength is randomly sampled from 1 to 20. We only train the newly added branches, with a learning rate of 1.0×10^{-4} over 10,000 steps.

Inference. During inference, we utilize the DDIM sampling process [57] with 25 denoising steps. Classifier-free guidance [24] is applied with a guidance scale set to 7.5. Following [70], we apply AdaIN [29] on latent videos for post-processing.

Computational Resources. Our experiments are conducted on a single GeForce RTX 3090 GPU using PyTorch, with a batch size of 1 on each GPU. We build upon the code-

base of AnimatedDiff [21]. Training takes approximately 36 hours per action.

A3.3. Evaluation Metrics

In line with previous works [23, 69, 70], we use three CLIP-based metrics to assess text alignment, image alignment, and temporal consistency. (1) *Text Alignment*: We compute the similarity between each frame and the provided text prompt, averaging the scores across all frames. (2) *Image Alignment*: Similar to Text Alignment, we replace the text prompt with the provided reference image to compute the image alignment score. (3) *Temporal Consistency*: We calculate the average similarity between consecutive frame pairs to obtain the temporal consistency score. We use ViT-L/14 from OpenAI [51] for feature extraction. In these three metrics, higher scores indicate better performance.

Following [72], we utilize Fréchet distance to compare generated and real videos. We use $CD-FVD$ [12] to mitigate content bias in the widely used FVD [62]. We use VideoMAE [61], pretrained on SomethingSomethingV2 [17], for feature extraction and calculate distance between real and generated videos. In this metric, lower distances reflect better performance.

To evaluate the similarity between generated and ground-truth videos in the HAA dataset, we calculate the cosine similarity for each pair of the generated and ground-truth videos. (1) *Cosine RGB*: We extract video features using I3D [3], pretrained on RGB videos, for both the generated and ground truth videos, calculating cosine similarity for each pair. (2) *Cosine Flow*: We extract optical flow using RAFT [60] and then use I3D [3], pretrained on optical flow data, to extract features for cosine similarity calculation. In these two metrics, higher similarities indicate better performance.

A3.4. Baselines

We compare FLASH with several image animation baselines: (1) T2V-Zero [48], a training-free image animation model based on a pretrained text-to-video model. (2) SparseCtrl [20], a model trained on large-scale datasets that encodes the reference image with a sparse condition encoder and integrates the features into a video generative model. (3) PIA [80], a model trained on large-scale datasets that incorporates the reference image into noisy latent videos. (4) DynamiCrafter [72], a model trained on large-scale datasets that injects the reference image features into generated videos via cross-attention layers and feature concatenation. (5) DreamVideo [68], which adapts subjects and motion using a limited set of samples; we customize motion for each action using the same training videos as FLASH. (6) LAMP [70], which learns motion patterns from a few videos; we train it with the same training videos as our method.

Instruction:

You will see a reference image on the left and seven human action videos on the right, all generated from that reference image and the same action description. Please carefully select the one video in each question that: (1) Best matches the action description and displays the action correctly and smoothly. (2) Maintains the overall appearance of the reference image on the left.

(1) Action Description: A person is drinking from a cup.



(2) Action Description: A person is doing a pushup.



Figure A4. AMT task interface.

Table A1. Analysis of training with fewer videos and joint training with multiple action classes.

Variant	# Videos Per Class	joint Training	Text Alignment (↑)	Image Alignment (↑)	Temporal Consistency (↑)	CD-FVD (↓)	Cosine RGB (↑)	Cosine Flow (↑)
#1	16	✗	22.53	77.10	95.43	1023.30	0.8380	0.6806
#2	16	✗	22.48	76.72	94.91	932.92	0.8398	0.7061
#5	16	✗	22.52	76.35	95.01	906.31	0.8446	0.7224
#1	8	✗	22.70	76.05	94.79	995.43	0.8250	0.6813
#2	8	✗	22.62	74.37	94.40	962.82	0.8330	0.7009
#5	8	✗	22.66	75.02	94.51	943.54	0.8340	0.7201
#1	4	✗	22.22	72.81	94.24	1050.03	0.8140	0.6802
#2	4	✗	22.60	72.00	93.83	1045.49	0.8188	0.7015
#5	4	✗	22.46	72.56	94.22	1031.87	0.8222	0.7183
#5	16	✗	22.52	76.35	95.01	906.31	0.8446	0.7224
#5	16	✓	22.61	77.47	95.39	897.05	0.8501	0.7232

A4. Results

A4.1. User Study

We conducted a user study on Amazon Mechanical Turk (AMT), where participants were asked to select the best generated video from a set of candidates. For each action, we randomly selected four different reference images and their corresponding generated videos for this user study. The AMT assessment interface, shown in Figure A4, presented workers with the following instructions: “You will see a reference image on the left and seven human action videos on the right, all generated from that reference image and an action description. Please carefully select the one video in each question that: (1) Best matches the action description and displays the action correctly and smoothly. (2) Maintains the overall appearance of the reference image on

the left.” The interface also displayed the reference image and action description.

To identify random clicking, each question was paired with a control question that included a real video of a randomly selected action, alongside clearly incorrect videos, such as static videos or videos from the same action class that did not match the reference image. Main and control questions were randomly shuffled within each question pair, and each pair was evaluated by 10 different workers. Responses from workers who failed the control questions were marked as invalid.

In total, we collected 366 valid responses. The preference rates for different methods are shown in the pie chart in Figure A5. FLASH was preferred in 67% of valid responses, significantly outperforming the next best choices, DynamiCrafter(14%) and LAMP (12%).

Table A2. Ablation studies on different values of τ for motion feature alignment, different values of p for inter-frame correspondence relation alignment, and the impact of the warping branch and patch attention branch in the Detail Enhancement Decoder.

Variant	τ	p	Warping Branch	Patch Attention Branch	Text Alignment (\uparrow)	Image Alignment (\uparrow)	Temporal Consistency (\uparrow)	CD-FVD (\downarrow)	Cosine RGB (\uparrow)	Cosine Flow (\uparrow)
#3	90	-	-	-	22.64	76.48	95.06	920.39	0.8444	0.7140
#3	75	-	-	-	22.58	76.63	95.16	904.25	0.8438	0.7119
#3	50	-	-	-	22.57	77.29	95.14	934.84	0.8430	0.7031
#3	25	-	-	-	22.33	76.52	94.85	930.53	0.8471	0.6979
#4	-	1.0	-	-	22.50	76.43	94.91	914.12	0.8422	0.6934
#4	-	0.5	-	-	22.70	76.31	94.84	938.21	0.8432	0.7172
#5	90	0.5	✗	✗	22.52	76.35	95.01	906.31	0.8446	0.7224
#6	90	0.5	✓	✗	22.54	76.21	95.35	918.61	0.8463	0.7196
#6	90	0.5	✗	✓	22.71	74.97	95.13	888.05	0.8332	0.7226
#6	90	0.5	✓	✓	22.77	76.22	95.31	908.39	0.8451	0.7233

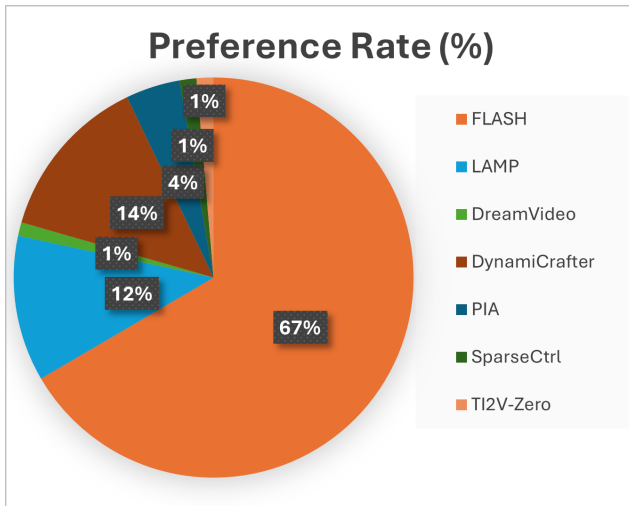


Figure A5. User preference rates (%) of different methods.

A4.2. Additional Ablation Studies

In line with the main paper, Variant #1 serves as the baseline, excluding both the Motion Alignment Module and the Detail Enhancement Decoder. Variant #2 uses only strongly augmented videos without any alignment technique. Variants #3, #4, and #5 progressively incorporate motion feature alignment, inter-frame correspondence relation alignment, and both, respectively. Lastly, Variant #6 builds upon Variant #5 by incorporating the Detail Enhancement Decoder.

Applicability with Fewer Training Videos. To assess the few-shot learning capability of the Motion Alignment Module, we conduct experiments using 8 and 4 videos randomly sampled from each action class. The results are shown in Table A1. We observe that Variant #5 consistently outper-

forms Variants #1 and #2 across different numbers of training videos per action class. The results validate that the Motion Alignment Module enhances the quality of animated videos in different few-shot configurations.

Joint Training with Multiple Action Classes. We examine whether the model benefits from joint training across multiple action classes. We use the training videos from the four action classes (sprint run, soccer shoot, canoeing sprint, and hugging human) to train a single model. The results in Table A1 show improvements across nearly all metrics. The improvements in Image Alignment, Temporal Consistency, and Cosine RGB are considerable. The results suggest that joint training with multiple action classes enhances the quality of the generated videos. This makes our technique more practical for applications that need to animate images to portray multiple delicate or customized human actions.

Analysis of Motion Alignment Module. In Table A2, we compare the performance of different τ values in Variant #3 and different p values in Variant #4. For τ , we observe that decreasing τ reduces performance in Temporal Consistency, CD-FVD, and Cosine Flow, especially in Temporal Consistency (94.85 for $\tau = 25$) and Cosine Flow (0.6979 for $\tau = 25$). This suggests that including more channels in motion features degrades video quality, likely because motion information is only encoded in a limited number of channels [71]. Thus, we set $\tau = 90$ for the remaining experiments. Regarding p , substituting inter-frame correspondence relations in all cross-frame attention layers ($p = 1.0$) lowers Cosine RGB and Cosine Flow (e.g., Cosine Flow drops to 0.6934 for $p = 1.0$). This might be due to the excessive regularization from substituting inter-frame correspondence relations in every layer, which makes learning difficult. Therefore, we use $p = 0.5$ in the remaining exper-



Figure A6. Failure cases.

iments.

Analysis of Detail Enhancement Decoder. In Table A2, we compare the effects of the Warping Branch and the Patch Attention Branch in Variant #6. Using only the Warping Branch leads to a notable improvement in Temporal Consistency (from 95.01 to 95.35). In contrast, the Patch Attention Branch provides a modest increase in Text Alignment (from 22.52 to 22.71) but results in a significant drop in Image Alignment (from 76.35 to 74.97). When both branches are combined, there is an enhancement in both Text Alignment and Temporal Consistency, accompanied by only a slight decrease in Image Alignment. These results suggest that the two branches have complementary effects.

A4.3. Experiments on UCF Sports Action Dataset

To evaluate the effectiveness of FLASH on additional datasets, we conducted experiments on the UCF Sports Action Dataset [59], focusing on two actions: golf swing and lifting. Due to the limited number of videos in this dataset, only 6 videos (golf swing) and 4 videos (lifting) are used for training.

Table A3 compares the performance of FLASH with baseline methods. FLASH achieves superior results on CD-FVD, Cosine RGB, and Cosine Flow, highlighting its ability to generate realistic motions. While DynamiCrafter performs better on Image Alignment and Temporal Consistency, this is primarily because it fails to animate the reference images and instead repeats it across frames, which represents a failure in animation. This limitation is further reflected in the poor scores of DynamiCrafter on CD-FVD and Cosine Flow. For Text Alignment, DreamVideo and T12V-Zero outperform FLASH, but their inability to generate smooth transitions from reference images is evident from their low Image Alignment scores. These observations, consistent with results on the HAA dataset, demonstrate the effectiveness of FLASH in scenarios with fewer training videos.

Table A3. Quantitative comparison of different methods on the UCF Sports Action Dataset.

Method	Text Alignment (↑)	Image Alignment (↑)	Temporal Consistency (↑)	CD-FVD (↓)	Cosine RGB (↑)	Cosine Flow (↑)
T12V-Zero	24.62	70.16	88.87	1222.35	0.7190	0.6443
SparseCtrl	23.26	61.16	89.69	1574.69	0.7156	0.6321
PIA	23.93	66.03	94.41	1385.54	0.7005	0.5851
DynamiCrafter	23.95	87.84	96.75	1630.83	<u>0.7783</u>	0.6316
DreamVideo	26.04	78.20	96.19	<u>949.72</u>	0.6860	0.7020
LAMP	24.02	81.17	95.17	1076.77	0.7415	<u>0.7378</u>
FLASH	24.11	<u>85.75</u>	<u>96.22</u>	480.70	0.8680	0.7936

A5. Limitations

Although FLASH can animate diverse reference images, it encounters challenges in accurately generating interactions involving human objects, particularly when multiple objects are present. For example, in Figure A6 (a), while a chopping action is depicted, the object being chopped is not the wood. Furthermore, if the initial action states in the reference images differ noticeably in motion details from those in the training videos, the model may struggle with animation. For example, in Figure A6 (b), the initial action status suggests a small-scale motion for chopping wood, which differs from the large-scale motion in training videos; in Figure A6 (c), the knee elevation motion contrasts with the steadier motion of running in place observed in the training videos; and in Figure A6 (d), a baby holding a cup with both hands deviates from the adult actions in the training videos, where one hand is used to hold the cup while drinking water. These results suggest that the model still lacks a thorough understanding of motion and interactions. Leveraging advanced multi-modal large language models to improve the understanding of human-object interactions could be a promising approach to addressing these challenges.

A6. Ethics Statement

We firmly oppose the misuse of generative AI for creating harmful content or spreading false information. We

do not assume any responsibility for potential misuse by users. Nonetheless, we recognize that our approach, which focuses on animation human images, carries the risk of potential misuse. To address these risks, we are committed to maintaining the highest ethical standards in our research by complying with legal requirements and protecting privacy. Additionally, we will explore implementing a content safety mechanism, similar to the one used in Stable Diffusion [54], as an effective way to address these concerns.

A7. Conclusion

In this paper, we introduce FLASH, a model that learns to animate images to depict human actions using minimal training data. We propose the Motion Alignment Module to learn consistent motion signals between videos with identical motion but different appearances, facilitating the learning of generalizable motion patterns. Additionally, we devise the Detail Enhancement Decoder to enhance details in generated frames, improving transition smoothness. Experimental results show that FLASH effectively animates diverse images with unseen actor or scene appearances, including those with unrealistic scenarios and humanoid aliens, into specified actions while maintaining smooth transitions.

References

- [1] Max Bain, Arsha Nagrani, Gül Varol, and Andrew Zisserman. Frozen in time: A joint video and image encoder for end-to-end retrieval. In *Proceedings of the IEEE/CVF International Conference on Computer Vision*, pages 1728–1738, 2021. 3
- [2] Andreas Blattmann, Robin Rombach, Huan Ling, Tim Dockhorn, Seung Wook Kim, Sanja Fidler, and Karsten Kreis. Align your latents: High-resolution video synthesis with latent diffusion models. In *Proceedings of the IEEE/CVF Conference on Computer Vision and Pattern Recognition*, pages 22563–22575, 2023. 2
- [3] Joao Carreira and Andrew Zisserman. Quo vadis, action recognition? a new model and the kinetics dataset. In *proceedings of the IEEE Conference on Computer Vision and Pattern Recognition*, pages 6299–6308, 2017. 12
- [4] Haoxin Chen, Yong Zhang, Xiaodong Cun, Menghan Xia, Xintao Wang, Chao Weng, and Ying Shan. Videocrafter2: Overcoming data limitations for high-quality video diffusion models. *arXiv preprint arXiv:2401.09047*, 2024. 2
- [5] Ricky TQ Chen, Jens Behrmann, David K Duvenaud, and Jörn-Henrik Jacobsen. Residual flows for invertible generative modeling. *Advances in Neural Information Processing Systems*, 32, 2019. 2
- [6] Tsai-Shien Chen, Aliaksandr Siarohin, Willi Menapace, Ekaterina Deyneka, Hsiang-wei Chao, Byung Eun Jeon, Yuwei Fang, Hsin-Ying Lee, Jian Ren, Ming-Hsuan Yang, et al. Panda-70m: Captioning 70m videos with multiple cross-modality teachers. In *Proceedings of the IEEE/CVF Conference on Computer Vision and Pattern Recognition*, pages 13320–13331, 2024. 3
- [7] Jihoon Chung, Cheng-hsin Wu, Hsuan-ru Yang, Yu-Wing Tai, and Chi-Keung Tang. Haa500: Human-centric atomic action dataset with curated videos. In *Proceedings of the IEEE/CVF international conference on computer vision*, pages 13465–13474, 2021. 2, 5, 11
- [8] Prafulla Dhariwal and Alexander Nichol. Diffusion models beat gans on image synthesis. *Advances in neural information processing systems*, 34:8780–8794, 2021. 3
- [9] Patrick Esser, Johnathan Chiu, Parmida Atighehchian, Jonathan Granskog, and Anastasis Germanidis. Structure and content-guided video synthesis with diffusion models. In *Proceedings of the IEEE/CVF International Conference on Computer Vision*, pages 7346–7356, 2023. 1, 3, 9
- [10] Patrick Esser, Sumith Kulal, Andreas Blattmann, Rahim Entezari, Jonas Müller, Harry Saini, Yam Levi, Dominik Lorenz, Axel Sauer, Frederic Boesel, et al. Scaling rectified flow transformers for high-resolution image synthesis. In *Forty-first International Conference on Machine Learning*, 2024. 7
- [11] Hao Fei, Shengqiong Wu, Wei Ji, Hanwang Zhang, and Tat-Seng Chua. Empowering dynamics-aware text-to-video diffusion with large language models. *arXiv preprint arXiv:2308.13812*, 2023. 2
- [12] Songwei Ge, Aniruddha Mahapatra, Gaurav Parmar, Jun-Yan Zhu, and Jia-Bin Huang. On the content bias in fréchet video distance. In *Proceedings of the IEEE/CVF Conference on Computer Vision and Pattern Recognition*, pages 7277–7288, 2024. 5, 12
- [13] Michal Geyer, Omer Bar-Tal, Shai Bagon, and Tali Dekel. Tokenflow: Consistent diffusion features for consistent video editing. *arXiv preprint arXiv:2307.10373*, 2023. 3
- [14] Rohit Girdhar, Mannat Singh, Andrew Brown, Quentin Duval, Samaneh Azadi, Sai Saketh Rambhatla, Akbar Shah, Xi Yin, Devi Parikh, and Ishan Misra. Emu video: Factorizing text-to-video generation by explicit image conditioning. *arXiv preprint arXiv:2311.10709*, 2023. 3
- [15] Litong Gong, Yiran Zhu, Weijie Li, Xiaoyang Kang, Biao Wang, Tiezheng Ge, and Bo Zheng. Atomovideo: High fidelity image-to-video generation. *arXiv preprint arXiv:2403.01800*, 2024. 1, 3
- [16] Ian Goodfellow, Jean Pouget-Abadie, Mehdi Mirza, Bing Xu, David Warde-Farley, Sherjil Ozair, Aaron Courville, and Yoshua Bengio. Generative adversarial networks. *Communications of the ACM*, 63(11):139–144, 2020. 2
- [17] Raghav Goyal, Samira Ebrahimi Kahou, Vincent Michalski, Joanna Materzynska, Susanne Westphal, Heuna Kim, Valentin Haenel, Ingo Fruend, Peter Yianilos, Moritz Mueller-Freitag, et al. The” something something” video database for learning and evaluating visual common sense. In *Proceedings of the IEEE international conference on computer vision*, pages 5842–5850, 2017. 12
- [18] Xianfan Gu, Chuan Wen, Weirui Ye, Jiaming Song, and Yang Gao. Seer: Language instructed video prediction with latent diffusion models. *arXiv preprint arXiv:2303.14897*, 2023. 2
- [19] Xun Guo, Mingwu Zheng, Liang Hou, Yuan Gao, Yufan Deng, Chongyang Ma, Weiming Hu, Zhengjun Zha, Haibin

- Huang, Pengfei Wan, et al. I2v-adapter: A general image-to-video adapter for video diffusion models. *arXiv preprint arXiv:2312.16693*, 2023. 1, 3
- [20] Yuwei Guo, Ceyuan Yang, Anyi Rao, Maneesh Agrawala, Dahua Lin, and Bo Dai. Sparsectrl: Adding sparse controls to text-to-video diffusion models. *arXiv preprint arXiv:2311.16933*, 2023. 1, 3, 5, 9, 12
- [21] Yuwei Guo, Ceyuan Yang, Anyi Rao, Yaohui Wang, Yu Qiao, Dahua Lin, and Bo Dai. Animatediff: Animate your personalized text-to-image diffusion models without specific tuning. *arXiv preprint arXiv:2307.04725*, 2023. 1, 2, 3, 9, 12
- [22] Yingqing He, Menghan Xia, Haoxin Chen, Xiaodong Cun, Yuan Gong, Jinbo Xing, Yong Zhang, Xintao Wang, Chao Weng, Ying Shan, et al. Animate-a-story: Storytelling with retrieval-augmented video generation. *arXiv preprint arXiv:2307.06940*, 2023. 1, 3, 11
- [23] Roberto Henschel, Levon Khachatryan, Daniil Hayrapetyan, Hayk Poghosyan, Vahram Tadevosyan, Zhangyang Wang, Shant Navasardyan, and Humphrey Shi. Streaming2v: Consistent, dynamic, and extendable long video generation from text. *arXiv preprint arXiv:2403.14773*, 2024. 5, 12
- [24] Jonathan Ho and Tim Salimans. Classifier-free diffusion guidance. *arXiv preprint arXiv:2207.12598*, 2022. 12
- [25] Jonathan Ho, Ajay Jain, and Pieter Abbeel. Denoising diffusion probabilistic models. *Advances in neural information processing systems*, 33:6840–6851, 2020. 2, 3
- [26] Jonathan Ho, William Chan, Chitwan Saharia, Jay Whang, Ruiqi Gao, Alexey Gritsenko, Diederik P Kingma, Ben Poole, Mohammad Norouzi, David J Fleet, et al. Imagen video: High definition video generation with diffusion models. *arXiv preprint arXiv:2210.02303*, 2022. 2
- [27] Jonathan Ho, Tim Salimans, Alexey Gritsenko, William Chan, Mohammad Norouzi, and David J Fleet. Video diffusion models. *Advances in Neural Information Processing Systems*, 35:8633–8646, 2022. 1, 2, 3, 9
- [28] Hanzhuo Huang, Yufan Feng, Cheng Shi, Lan Xu, Jingyi Yu, and Sibe Yang. Free-bloom: Zero-shot text-to-video generator with llm director and ldm animator. *Advances in Neural Information Processing Systems*, 36, 2024. 2
- [29] Xun Huang and Serge Belongie. Arbitrary style transfer in real-time with adaptive instance normalization. In *Proceedings of the IEEE international conference on computer vision*, pages 1501–1510, 2017. 12
- [30] Ziqi Huang, Tianxing Wu, Yuming Jiang, Kelvin CK Chan, and Ziwei Liu. Reversion: Diffusion-based relation inversion from images. *arXiv preprint arXiv:2303.13495*, 2023. 11
- [31] Hyeonho Jeong, Geon Yeong Park, and Jong Chul Ye. Vmc: Video motion customization using temporal attention adaptation for text-to-video diffusion models. In *Proceedings of the IEEE/CVF Conference on Computer Vision and Pattern Recognition*, pages 9212–9221, 2024. 3
- [32] Yuming Jiang, Tianxing Wu, Shuai Yang, Chenyang Si, Dahua Lin, Yu Qiao, Chen Change Loy, and Ziwei Liu. Videobooth: Diffusion-based video generation with image prompts. *arXiv preprint arXiv:2312.00777*, 2023. 1, 3
- [33] Hitesh Kandala, Jianfeng Gao, and Jianwei Yang. Pix2gif: Motion-guided diffusion for gif generation. *arXiv preprint arXiv:2403.04634*, 2024. 1, 3
- [34] Manuel Kansy, Jacek Naruniec, Christopher Schroers, Markus Gross, and Romann M Weber. Reenact anything: Semantic video motion transfer using motion-textual inversion. *arXiv preprint arXiv:2408.00458*, 2024. 1, 3
- [35] Levon Khachatryan, Andranik Movsisyan, Vahram Tadevosyan, Roberto Henschel, Zhangyang Wang, Shant Navasardyan, and Humphrey Shi. Text2video-zero: Text-to-image diffusion models are zero-shot video generators. *arXiv preprint arXiv:2303.13439*, 2023. 3, 9
- [36] Diederik P Kingma and Max Welling. Auto-encoding variational bayes. *arXiv preprint arXiv:1312.6114*, 2013. 2
- [37] Xiaomin Li, Xu Jia, Qinghe Wang, Haiwen Diao, Pengxiang Li, You He, Huchuan Lu, et al. Motrans: Customized motion transfer with text-driven video diffusion models. In *ACM Multimedia 2024*, 2024. 1, 3
- [38] Yumeng Li, William Beluch, Margret Keuper, Dan Zhang, and Anna Khoreva. Vstar: Generative temporal nursing for longer dynamic video synthesis. *arXiv preprint arXiv:2403.13501*, 2024. 2
- [39] Long Lian, Baifeng Shi, Adam Yala, Trevor Darrell, and Boyi Li. Llm-grounded video diffusion models. *arXiv preprint arXiv:2309.17444*, 2023. 3
- [40] Jun Hao Liew, Hanshu Yan, Jianfeng Zhang, Zhongcong Xu, and Jiashi Feng. Magicedit: High-fidelity and temporally coherent video editing. *arXiv preprint arXiv:2308.14749*, 2023. 1, 3
- [41] Pengyang Ling, Jiayi Bu, Pan Zhang, Xiaoyi Dong, Yuhang Zang, Tong Wu, Huaian Chen, Jiaqi Wang, and Yi Jin. Motionclone: Training-free motion cloning for controllable video generation. *arXiv preprint arXiv:2406.05338*, 2024. 3
- [42] Yu Lu, Linchao Zhu, Hehe Fan, and Yi Yang. Flowzero: Zero-shot text-to-video synthesis with llm-driven dynamic scene syntax. *arXiv preprint arXiv:2311.15813*, 2023. 3
- [43] Jiaxi Lv, Yi Huang, Mingfu Yan, Jiancheng Huang, Jianzhuang Liu, Yifan Liu, Yafei Wen, Xiaoxin Chen, and Shifeng Chen. Gpt4motion: Scripting physical motions in text-to-video generation via blender-oriented gpt planning. In *Proceedings of the IEEE/CVF Conference on Computer Vision and Pattern Recognition*, pages 1430–1440, 2024. 3
- [44] Yue Ma, Yingqing He, Hongfa Wang, Andong Wang, Chenyang Qi, Chengfei Cai, Xiu Li, Zhifeng Li, Heung-Yeung Shum, Wei Liu, et al. Follow-your-click: Open-domain regional image animation via short prompts. *arXiv preprint arXiv:2403.08268*, 2024. 1, 3
- [45] Arun Mallya, Ting-Chun Wang, and Ming-Yu Liu. Implicit warping for animation with image sets. *Advances in Neural Information Processing Systems*, 35:22438–22450, 2022. 5
- [46] Joanna Materzynska, Josef Sivic, Eli Shechtman, Antonio Torralba, Richard Zhang, and Bryan Russell. Customizing motion in text-to-video diffusion models. *arXiv preprint arXiv:2312.04966*, 2023. 1, 3, 11
- [47] Haomiao Ni, Changhao Shi, Kai Li, Sharon X Huang, and Martin Renqiang Min. Conditional image-to-video generation with latent flow diffusion models. In *Proceedings of*

- the *IEEE/CVF Conference on Computer Vision and Pattern Recognition*, pages 18444–18455, 2023. 1, 3
- [48] Haomiao Ni, Bernhard Egger, Suhas Lohit, Anoop Cherian, Ye Wang, Toshiaki Koike-Akino, Sharon X Huang, and Tim K Marks. Ti2v-zero: Zero-shot image conditioning for text-to-video diffusion models. In *Proceedings of the IEEE/CVF Conference on Computer Vision and Pattern Recognition*, pages 9015–9025, 2024. 5, 12
- [49] Geon Yeong Park, Hyeonho Jeong, Sang Wan Lee, and Jong Chul Ye. Spectral motion alignment for video motion transfer using diffusion models. *arXiv preprint arXiv:2403.15249*, 2024. 3
- [50] Chenyang Qi, Xiaodong Cun, Yong Zhang, Chenyang Lei, Xintao Wang, Ying Shan, and Qifeng Chen. Fatezero: Fusing attentions for zero-shot text-based video editing. In *Proceedings of the IEEE/CVF International Conference on Computer Vision*, pages 15932–15942, 2023. 3
- [51] Alec Radford, Jong Wook Kim, Chris Hallacy, Aditya Ramesh, Gabriel Goh, Sandhini Agarwal, Girish Sastry, Amanda Askell, Pamela Mishkin, Jack Clark, et al. Learning transferable visual models from natural language supervision. In *International conference on machine learning*, pages 8748–8763. PMLR, 2021. 12
- [52] Weiming Ren, Harry Yang, Ge Zhang, Cong Wei, Xinrun Du, Stephen Huang, and Wenhui Chen. Consisti2v: Enhancing visual consistency for image-to-video generation. *arXiv preprint arXiv:2402.04324*, 2024. 1, 3, 9, 11
- [53] Yixuan Ren, Yang Zhou, Jimei Yang, Jing Shi, Difan Liu, Feng Liu, Mingi Kwon, and Abhinav Shrivastava. Customize-a-video: One-shot motion customization of text-to-video diffusion models. *arXiv preprint arXiv:2402.14780*, 2024. 3
- [54] Robin Rombach, Andreas Blattmann, Dominik Lorenz, Patrick Esser, and Björn Ommer. High-resolution image synthesis with latent diffusion models. In *Proceedings of the IEEE/CVF conference on computer vision and pattern recognition*, pages 10684–10695, 2022. 3, 16
- [55] Xiaoyu Shi, Zhaoyang Huang, Fu-Yun Wang, Weikang Bian, Dasong Li, Yi Zhang, Manyuan Zhang, Ka Chun Cheung, Simon See, Hongwei Qin, et al. Motion-i2v: Consistent and controllable image-to-video generation with explicit motion modeling. *arXiv preprint arXiv:2401.15977*, 2024. 1, 3
- [56] Uriel Singer, Adam Polyak, Thomas Hayes, Xi Yin, Jie An, Songyang Zhang, Qiyuan Hu, Harry Yang, Oron Ashual, Oran Gafni, et al. Make-a-video: Text-to-video generation without text-video data. *arXiv preprint arXiv:2209.14792*, 2022. 1, 2
- [57] Jiaming Song, Chenlin Meng, and Stefano Ermon. Denoising diffusion implicit models. *arXiv preprint arXiv:2010.02502*, 2020. 2, 12
- [58] Yang Song, Jascha Sohl-Dickstein, Diederik P Kingma, Abhishek Kumar, Stefano Ermon, and Ben Poole. Score-based generative modeling through stochastic differential equations. *arXiv preprint arXiv:2011.13456*, 2020. 2
- [59] Khurram Soomro and Amir R Zamir. Action recognition in realistic sports videos. In *Computer vision in sports*, pages 181–208. Springer, 2015. 15
- [60] Zachary Teed and Jia Deng. Raft: Recurrent all-pairs field transforms for optical flow. In *Computer Vision—ECCV 2020: 16th European Conference, Glasgow, UK, August 23–28, 2020, Proceedings, Part II 16*, pages 402–419. Springer, 2020. 12
- [61] Zhan Tong, Yibing Song, Jue Wang, and Limin Wang. Videomae: Masked autoencoders are data-efficient learners for self-supervised video pre-training. *Advances in neural information processing systems*, 35:10078–10093, 2022. 12
- [62] Thomas Unterthiner, Sjoerd Van Steenkiste, Karol Kurach, Raphael Marinier, Marcin Michalski, and Sylvain Gelly. Towards accurate generative models of video: A new metric & challenges. *arXiv preprint arXiv:1812.01717*, 2018. 5, 12
- [63] Cong Wang, Jiaxi Gu, Panwen Hu, Songcen Xu, Hang Xu, and Xiaodan Liang. Dreamvideo: High-fidelity image-to-video generation with image retention and text guidance. *arXiv preprint arXiv:2312.03018*, 2023. 1, 3
- [64] Jiawei Wang, Yuchen Zhang, Jiaxin Zou, Yan Zeng, Guoqiang Wei, Liping Yuan, and Hang Li. Boximator: Generating rich and controllable motions for video synthesis. *arXiv preprint arXiv:2402.01566*, 2024. 1, 3
- [65] Wenjing Wang, Huan Yang, Zixi Tuo, Huiguo He, Junchen Zhu, Jianlong Fu, and Jiaying Liu. Videofactory: Swap attention in spatiotemporal diffusions for text-to-video generation. *arXiv preprint arXiv:2305.10874*, 2023. 2
- [66] Xiang Wang, Hangjie Yuan, Shiwei Zhang, Dayou Chen, Junyi Wang, Yingya Zhang, Yujun Shen, Deli Zhao, and Jingren Zhou. Videocomposer: Compositional video synthesis with motion controllability. *Advances in Neural Information Processing Systems*, 36, 2024. 1, 3
- [67] Yanhui Wang, Jianmin Bao, Wenming Weng, Ruoyu Feng, Dacheng Yin, Tao Yang, Jingxu Zhang, Qi Dai, Zhiyuan Zhao, Chunyu Wang, et al. Microcinema: A divide-and-conquer approach for text-to-video generation. In *Proceedings of the IEEE/CVF Conference on Computer Vision and Pattern Recognition*, pages 8414–8424, 2024. 3
- [68] Yujie Wei, Shiwei Zhang, Zhiwu Qing, Hangjie Yuan, Zhiheng Liu, Yu Liu, Yingya Zhang, Jingren Zhou, and Hongming Shan. Dreamvideo: Composing your dream videos with customized subject and motion. In *Proceedings of the IEEE/CVF Conference on Computer Vision and Pattern Recognition*, pages 6537–6549, 2024. 1, 3, 5, 12
- [69] Jay Zhangjie Wu, Yixiao Ge, Xintao Wang, Stan Weixian Lei, Yuchao Gu, Yufei Shi, Wynne Hsu, Ying Shan, Xiaohu Qie, and Mike Zheng Shou. Tune-a-video: One-shot tuning of image diffusion models for text-to-video generation. In *Proceedings of the IEEE/CVF International Conference on Computer Vision*, pages 7623–7633, 2023. 1, 3, 5, 12
- [70] Ruiqi Wu, Liangyu Chen, Tong Yang, Chunle Guo, Chongyi Li, and Xiangyu Zhang. Lamp: Learn a motion pattern for few-shot-based video generation. *arXiv preprint arXiv:2310.10769*, 2023. 1, 3, 5, 9, 11, 12
- [71] Zeqi Xiao, Yifan Zhou, Shuai Yang, and Xingang Pan. Video diffusion models are training-free motion interpreter and controller. *arXiv preprint arXiv:2405.14864*, 2024. 4, 14
- [72] Jinbo Xing, Menghan Xia, Yong Zhang, Haoxin Chen, Xintao Wang, Tien-Tsin Wong, and Ying Shan. Dynamicrafter:

- Animating open-domain images with video diffusion priors. *arXiv preprint arXiv:2310.12190*, 2023. [1](#), [3](#), [5](#), [12](#)
- [73] Hongwei Xue, Tiankai Hang, Yanhong Zeng, Yuchong Sun, Bei Liu, Huan Yang, Jianlong Fu, and Baining Guo. Advancing high-resolution video-language representation with large-scale video transcriptions. In *Proceedings of the IEEE/CVF Conference on Computer Vision and Pattern Recognition*, pages 5036–5045, 2022. [3](#)
- [74] Shuai Yang, Yifan Zhou, Ziwei Liu, and Chen Change Loy. Rerender a video: Zero-shot text-guided video-to-video translation. In *SIGGRAPH Asia 2023 Conference Papers*, pages 1–11, 2023. [3](#)
- [75] Xiangpeng Yang, Linchao Zhu, Hehe Fan, and Yi Yang. Eva: Zero-shot accurate attributes and multi-object video editing. *arXiv preprint arXiv:2403.16111*, 2024. [3](#)
- [76] Shengming Yin, Chenfei Wu, Jian Liang, Jie Shi, Houqiang Li, Gong Ming, and Nan Duan. Dragnuwa: Fine-grained control in video generation by integrating text, image, and trajectory. *arXiv preprint arXiv:2308.08089*, 2023. [1](#), [3](#)
- [77] Yan Zeng, Guoqiang Wei, Jiani Zheng, Jiaxin Zou, Yang Wei, Yuchen Zhang, and Hang Li. Make pixels dance: High-dynamic video generation. *arXiv preprint arXiv:2311.10982*, 2023. [3](#)
- [78] Jianfeng Zhang, Hanshu Yan, Zhongcong Xu, Jiashi Feng, and Jun Hao Liew. Magicavatar: Multimodal avatar generation and animation. *arXiv preprint arXiv:2308.14748*, 2023. [1](#), [3](#)
- [79] Yuxin Zhang, Fan Tang, Nisha Huang, Haibin Huang, Chongyang Ma, Weiming Dong, and Changsheng Xu. Motioncrafter: One-shot motion customization of diffusion models. *arXiv preprint arXiv:2312.05288*, 2023. [3](#)
- [80] Yiming Zhang, Zhening Xing, Yanhong Zeng, Youqing Fang, and Kai Chen. Pia: Your personalized image animator via plug-and-play modules in text-to-image models. *arXiv preprint arXiv:2312.13964*, 2023. [1](#), [5](#), [12](#)
- [81] Rui Zhao, Yuchao Gu, Jay Zhangjie Wu, David Junhao Zhang, Jiawei Liu, Weijia Wu, Jussi Keppo, and Mike Zheng Shou. Motiondirector: Motion customization of text-to-video diffusion models. *arXiv preprint arXiv:2310.08465*, 2023. [1](#), [3](#)
- [82] Daquan Zhou, Weimin Wang, Hanshu Yan, Weiwei Lv, Yizhe Zhu, and Jiashi Feng. Magicvideo: Efficient video generation with latent diffusion models. *arXiv preprint arXiv:2211.11018*, 2022. [1](#), [2](#)